Sensorless Control for Induction Machines Using Square-wave Voltage Injection

Young-doo Yoon
Member, IEEE
Samsung Electronics
Suwon, Korea
youngdoo.yoon@gmail.com

Seung-ki Sul
Fellow, IEEE
Seoul National University
Seoul, Korea
sulsk@plaza.snu.ac.kr

***Abstract* -- This paper presents a sensorless control for induction machines using a square-wave voltage injection. Multiple saliencies and a saliency orientation shift are considered in this paper. The multiple saliencies make the position error signal distorted and the estimation of the flux position difficult. And, due to the saliency orientation shift, the estimated rotor flux position drifts from the actual rotor flux position according to torque and speed. When the square-wave voltage is injected into the estimated synchronous reference d-q frame, the error signal has lower harmonics than that of the conventional sinusoidal injection method. In addition, by injecting the square-wave into q axis of the estimated synchronous reference frame, the flux can be estimated with less error compared to the injection into d axis. Because of the enhanced rotor flux estimation performance, the square wave injection into q axis reveals better torque controllability compared to the sine wave injection into d axis.**

***Index Terms*—AC machines, induction machine, sensorless control, signal injection, square-wave voltage**

I. INTRODUCTION

The application areas of sensorless drives of AC motors are being widespread from industrial applications to electric home appliances to take advantages such as cost, size and reliability of systems [1], [2]. Many sensorless techniques have been studied and these techniques can be classified into two categories: techniques based on back-EMF [3] and techniques based on saliency in spatial impedance of the motor [4]-[11].

The former uses voltage models [3] and/or observers. It presents good results in the medium and high speed regions. However, it cannot keep the performance in the zero and/or low speed region where the back EMF disappears. The latter exploits the magnetic saliency. Some algorithms inject test voltage signals in a sampling period to estimate rotor position [4]. However, they can be frail to parameter variation or measurement noises since they detect inductance difference using test voltage signals in a short time. High frequency injection methods were proposed and there are two approaches: rotating signal injection method at the stationary reference frame [6] and pulsating signal injection method at the estimated synchronous reference frame [7]-[9]. These methods can be applied to general AC machines and they show reasonable torque control capability at zero and/or low frequency, even under heavily loaded condition. Recently, square-wave voltage injection methods in [10], [11] have been proposed. Due to the square-wave injection scheme, the position error signal of them can be calculated without any Low Pass Filters (LPF), and that means that it could obtained without time delay, which is crucial to extend the bandwidth of the sensorless control. Hence, the position estimation performance can be enhanced remarkably. Also, the higher injection frequency can be utilized and the injection frequency has been definitely separated from the fundamental frequency of the motor. As the result, the square wave injection method reveals better sensorless drive performance compared to the conventional method injecting sinusoidal voltage signals.

Generally, the sensorless control of the Induction Machines (IMs) with the high frequency signal injection exploits the impedance saliency of IMs due to the magnetic saturation. But multiple saliencies [12] and saliency orientation shift [13] occur with the injected signal. The multiple saliencies of the induction machines make the position error signal distorted and estimation of the rotor flux position difficult. And, due to the saliency orientation shift, the estimated rotor flux deviates from actual rotor flux position according to the operating conditions, and a compensation scheme is inevitable to keep the torque controllability.

In this paper, sensorless control for induction machines using a square-wave voltage injection is presented. When the square-wave voltage is injected, the error signal has less harmonics compared to the conventional sinusoidal signal injection. In addition, through injecting the square-wave into q axis of the estimated synchronous d-q frame, the saliency orientation shift becomes smaller compared to injecting the signal into d axis. As a consequence, the robustness of the sensorless control of induction machines to operating condition is enhanced compared to the conventional sinusoidal voltage injection method.

II. SENSORLESS ALGORITHM BASED ON SQUARE-WAVE VOLTAGE INJECTION METHOD FOR IMS

Sensorless algorithms [6], [7] based on high frequency injection method exploit the saliency of induction machines at the injected high frequency. Using this saliency with the high frequency injection method, sensorless algorithms can extract rotor flux information even at zero stator frequency.

978-1-4244-5287-3/10/$26.00 ©2010 IEEE

All the high frequency voltage signal injection methods for the sensorless control of IMs rely on the induced high frequency current in the stationary reference frame, i^s_{dqsh}, which is the only measurable quantity. So, i^s_{dqsh} should be analyzed according to voltage injection methods. In here, for the convenience of the derivation of equations, it is assumed that the square-wave voltage is injected into d-axis of the synchronous reference frame [10]. However, if the signal is injected into q axis, the equations can be derived similarly.

The injected high frequency voltage can be described as (1) with the assumption of that the estimation error of rotor flux position ($\tilde{\theta}_e = \theta_e - \hat{\theta}_e$) is small enough.

$$V^{\hat{e}}_{dsh} = \begin{cases} V_{inj}, & half\ duty \\ -V_{inj}, & otherwise \end{cases},\ V^{\hat{e}}_{qsh} = 0,\ \tilde{\theta}_e = \theta_e - \hat{\theta}_e \approx 0 \quad (1)$$

where V_{inj} is the magnitude of the injected voltage. Considering the relationship between the induced high frequency current and the injected voltage, the high frequency current can be described as (2).

$$\begin{bmatrix} i^s_{dsh} \\ i^s_{qsh} \end{bmatrix} = \left[R(\theta_e)\right]^{-1}\left[Z^e\right]^{-1}\begin{bmatrix} v^e_{dsh} \\ v^e_{qsh} \end{bmatrix} = \left[R(\theta_e)\right]^{-1}\left[Z^e\right]^{-1}\left[R(\tilde{\theta}_e)\right]\begin{bmatrix} v^{\hat{e}}_{dsh} \\ v^{\hat{e}}_{qsh} \end{bmatrix} \quad . (2)$$

The reactances, $\omega_h L^e_{dh}$ and $\omega_h L^e_{qh}$ are generally much larger than R^e_{dh} and R^e_{qh} in the high frequency impedance model. And, the injected frequency, ω_h, is also at least one order larger than the fundamental frequency, ω_r. Therefore, high frequency impedance in the synchronous reference frame, Z^e, can be simplified as follows.

$$\left[Z^e\right] = \begin{bmatrix} R^e_{dh} + L^e_{dh}\cdot s & -\omega_e L^r_{qh} \\ \omega_e L^e_{dh} & R^e_{qh} + L^e_{qh}\cdot s \end{bmatrix} \approx \begin{bmatrix} L^e_{dh}\cdot s & 0 \\ 0 & L^e_{qh}\cdot s \end{bmatrix}. \quad (3)$$

When the square-wave type voltage in (1) is injected, corresponding Δi^s_{dqsh} which stands for the difference between previous and present sampled currents can be simply described as (4) under the assumption of (5).

$$\begin{bmatrix} \Delta i^s_{dsh} \\ \Delta i^s_{qsh} \end{bmatrix} \approx \begin{bmatrix} \cos(\theta_e) & -\sin(\theta_e) \\ \sin(\theta_e) & \cos(\theta_e) \end{bmatrix}\begin{bmatrix} \dfrac{\cos(\tilde{\theta}_e)V^{\hat{e}}_{dsh}\Delta T}{L^e_{dh}} \\ \dfrac{-\sin(\tilde{\theta}_e)V^{\hat{e}}_{dsh}\Delta T}{L^e_{qh}} \end{bmatrix} = V^{\hat{e}}_{dsh}\Delta T\begin{bmatrix} \dfrac{\cos(\theta_e)\cos(\tilde{\theta}_e)}{L^e_{dh}} + \dfrac{\sin(\theta_e)\sin(\tilde{\theta}_e)}{L^e_{qh}} \\ \dfrac{\sin(\theta_e)\cos(\tilde{\theta}_e)}{L^e_{dh}} - \dfrac{\cos(\theta_e)\sin(\tilde{\theta}_e)}{L^e_{qh}} \end{bmatrix} \quad (4)$$

$$\left[Z^e\right]^{-1} \approx \begin{bmatrix} \dfrac{1}{L^e_{dh}\cdot s} & 0 \\ 0 & \dfrac{1}{L^e_{qh}\cdot s} \end{bmatrix} \quad (5)$$

where ΔT means the sampling period. To consider the polarity of the injected voltage, a signal noted by $\Delta i^s_{dqsh}{}'$ is defined as (6). Then, Δi^s_{dqsh} can be modified as (7).

$$\Delta i^s_{dsh}{}' = \begin{cases} \Delta i^s_{dsh}, if\ V^{\hat{e}}_{dsh} > 0 \\ -\Delta i^s_{dsh}, otherwise \end{cases}, \Delta i^s_{qsh}{}' = \begin{cases} \Delta i^s_{qsh}, if\ V^{\hat{e}}_{dsh} > 0 \\ -\Delta i^s_{qsh}, otherwise \end{cases} \quad (6)$$

$$\begin{bmatrix} \Delta i^s_{dsh}{}' \\ \Delta i^s_{qsh}{}' \end{bmatrix} = V_{inj}\Delta T\cdot\begin{bmatrix} \dfrac{\cos(\theta_e)\cos(\tilde{\theta}_e)}{L^e_{dh}} + \dfrac{\sin(\theta_e)\sin(\tilde{\theta}_e)}{L^e_{qh}} \\ \dfrac{\sin(\theta_e)\cos(\tilde{\theta}_e)}{L^e_{dh}} - \dfrac{\cos(\theta_e)\sin(\tilde{\theta}_e)}{L^e_{qh}} \end{bmatrix} \approx V_{inj}\Delta T\cdot\begin{bmatrix} \dfrac{\cos(\theta_e)}{L^r_{dh}} \\ \dfrac{\sin(\theta_e)}{L^r_{dh}} \end{bmatrix} \text{(Under assumption that } \tilde{\theta}_e \approx 0\text{).} \quad (7)$$

As shown in (7), $\Delta i^s_{dqsh}{}'$ directly represents the rotor flux position, θ_e. $\Delta i^s_{dsh}{}'$ and $\Delta i^s_{qsh}{}'$ show the cosine and sine function of the rotor flux position, respectively. Therefore, using arctangent function, the rotor flux position, θ_{eCal} can be calculated from $\Delta i^s_{dqsh}{}'$, as (8), and the error signal of the position state filter, $f(\tilde{\theta}_e)$, can be represented from θ_{eCal} as (9). θ_{eCal} and $f(\tilde{\theta}_e)$ can be obtained at every sampling instant with no LPF and that means that the position error signal could be obtained with no time delay. Using a state filter with the error signal, $f(\tilde{\theta}_e)$, $\hat{\theta}_e$ can be obtained.

TABLE I
NOMINAL PARAMETERS OF MOTOR UNDER THE TEST

Quantity	Value [Unit]
Rated Power	11 [kW]
Rated Speed	1750 [r/min]
Rated Torque	60 [Nm]
Rated Line Frequency	59.6 [Hz]
Number of Pole	4
Rated Line Voltage	180 [V_{RMS}]
Rated Current	45 [A_{RMS}]

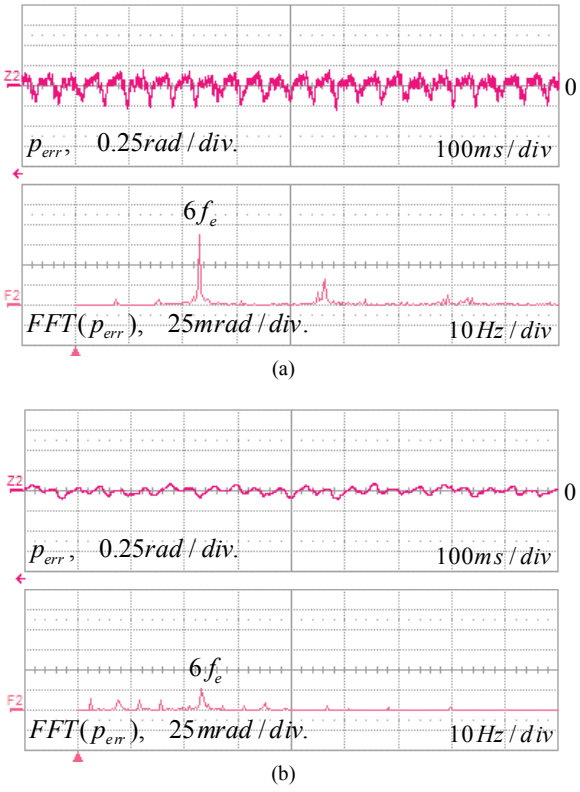

Fig. 1 Position estimation error signals and their FFT results under 50 % of the rated torque: (a) with the conventional synchronous pulsating signal injection method and (b) with the square-wave signal injection method.

$$\theta_{eCal} = \text{atan2}\left(\Delta i_{qsh}^{s}{}', \Delta i_{dsh}^{s}{}' \right) \tag{8}$$

$$f(\tilde{\theta}_e) \equiv \theta_{eCal} - \hat{\theta}_e \approx K_{error}\tilde{\theta}_e \qquad \left(\tilde{\theta}_e \approx 0\right) \tag{9}$$

III. THE PROPOSED SENSORLESS ALGORITHM

The injected high frequency signal introduces high frequency flux linkage through the leakage flux paths and these leakage paths become saturated with the high frequency flux and the main flux. Actually, machines have a number of localized leakage flux paths and they are also saturated [14]. Due to these localized saturations, the multiple saliencies occur and the estimated position of the rotor flux would not be the real one by the rotor flux linkage but the locally saturated position by the leakage flux.

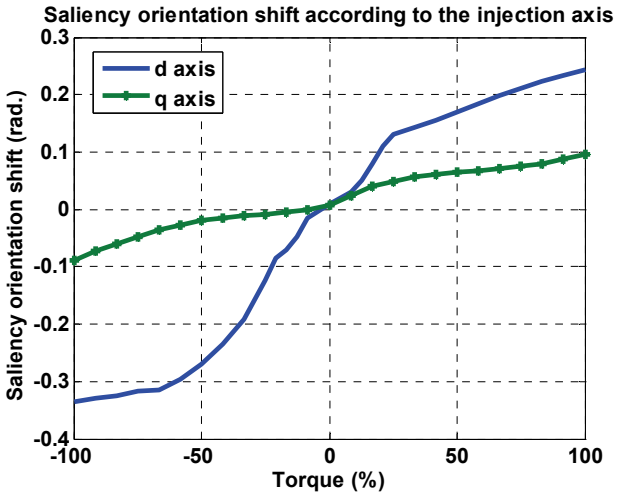

Fig. 2 Compensation angle according to the injection axis and the torque.

In order to clearly demonstrate the multiple saliencies, the position estimation error was experimentally measured by running the induction machine under sensored indirect rotor flux orientation (IRFO) control of 100 r/min. The nominal parameters of the machine under test are listed as Table I. Fig. 1 shows the position error signals and their FFT results under 50 % of the rated torque. Fig. 1(a) and Fig. 1(b) demonstrate those with the conventional pulsating sinusoidal signal injection method and the square-wave signal injection method, respectively. As shown in the figure, the results in Fig. 1(b) show lower harmonics than those in Fig. 1(a). As shown in the figure, the multiple saliency problems can be overcome by injecting square-wave signal into the estimated synchronous reference frame.

However, the position of the high frequency saliency by the rotor flux linkage also shifts according to the load conditions. The multiple saliency problems can be minimized by injecting square-wave signal into the estimated d or q axis of the d-q synchronous reference frame and the error signal may be robust to the local saliency since it comes near the saliency point of the rotor flux linkage. Still, however, the estimated position from the error signal should be compensated according to the load due to the Saliency Orientation Shift (SOS). The compensation angle for SOS can be identified by off-line test of IMs by running the induction machine under sensored IRFO control, and the estimated rotor flux position by the injected square wave signal is monitored and compared to the angle by sensored IRFO angle.

In Fig. 2, the compensation angle, $\varphi = \theta_{e,IRFO} - \hat{\theta}_{e,SAT}$, is shown according to d axis injection and q axis injection. Then the angle of the rotor flux for the field orientation control can be obtained as (9).

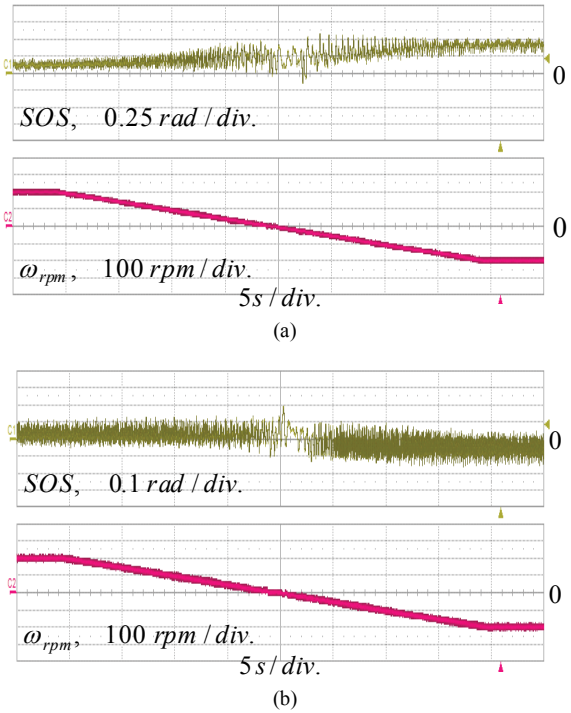

Fig. 3 Compensation angle according to the rotating speed under 50 % of the rated torque: (a) with d axis injection and (b) with q axis injection.

$$\hat{\theta}_e = \hat{\theta}_{e,SAT} + \varphi(i_{qs}^{e*}) \tag{9}$$

where $\hat{\theta}_{e,SAT}$ represents the estimated position of the rotor flux linkage by the square-wave signal injection. As shown in Fig. 2, the angle in q axis injection is much smaller than that in d axis injection. Though Fig. 2 shows the compensation angle under the square-wave signal injection, it also appears under the sinusoidal signal injection as common phenomena of injection schemes.

Additionally, the compensation angle also depends not only on the load condition but also on the operating speed. Fig. 3 shows SOS according to speed. As shown in Fig. 3, again, SOS in q axis injection is much smaller than that in d axis injection. Therefore, using q axis injection, the compensation angle would be smaller in overall operating conditions, and the estimation of the angle is robust to the torque and speed variations. And in this case the compensation angle could be easily obtained as a simple one dimensional look-up table or a simplified function. In experiments, it is simply implemented as a linear function of i_{qs}^{e*}.

IV. Experimental Results

Experiments with a general purpose Induction Machine (IM) were performed to verify the effectiveness of the proposed method. The induction machine is coupled to a permanent magnet synchronous servo motor as a load machine. The induction machine under the test is an 11-kW four-pole closed-slot skewed-rotor machine. The nominal parameters of the machine under test are listed as Table I. The square-wave voltage was injected into q axis of the estimated synchronous d-q frame. The induction machine was driven by the proposed sensorless speed control and the load machine was driven by torque control.

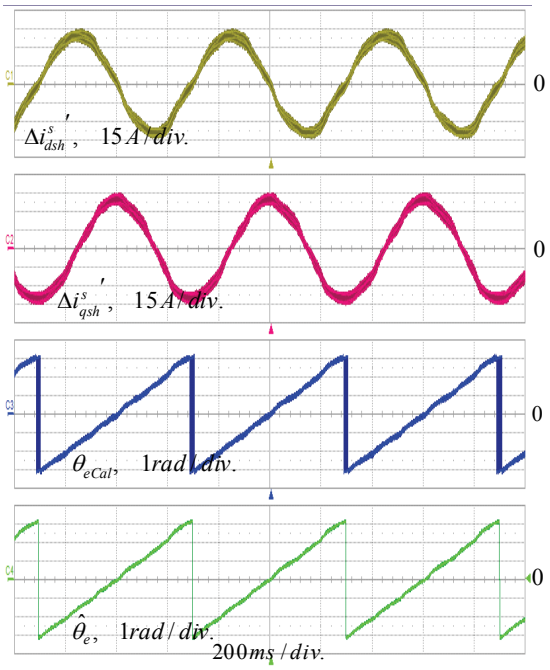

Fig. 4 Rotor flux position estimation performance.

Fig. 4 shows the rotor flux position estimation performance of the proposed sensorless control under constant speed operation of 50 r/min. $\Delta i_{dqsh}^{s\prime}$, θ_{eCal} and $\hat{\theta}_e$ are demonstrated together. In (7) of the previous chapter where the voltage signal is injected in the d axis of the estimated synchronous d-q frame, $\Delta i_{dsh}^{s\prime}$ and $\Delta i_{qsh}^{s\prime}$ show the cosine and sine function of the rotor flux position, respectively. In here, however, $\Delta i_{dsh}^{s\prime}$ and $\Delta i_{qsh}^{s\prime}$ show the forms of $-\sin\hat{\theta}_e$ and $\cos\hat{\theta}_e$, respectively. This is because the voltage signal is injected in the q axis. With an arctangent function and $\Delta i_{dqsh}^{s\prime}$, θ_{eCal} is calculated and then, $\hat{\theta}_e$ is obtained through a state filter. As shown in this figure, the flux position can be clearly estimated.

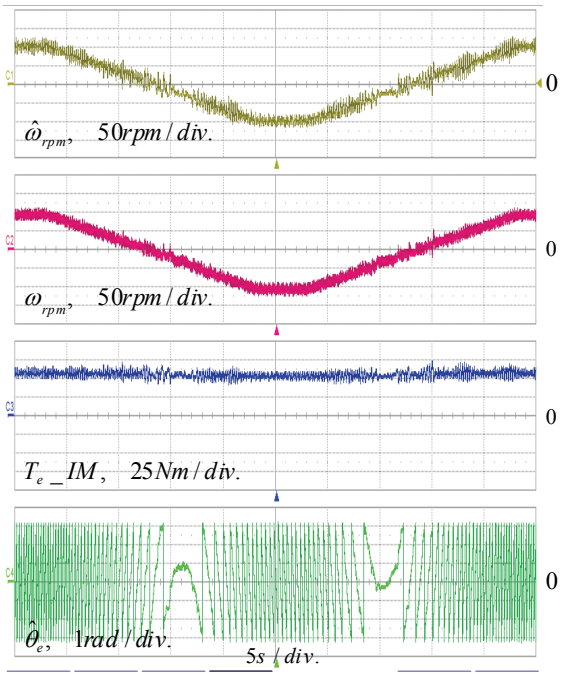

Fig. 5 Slow speed reversal under the rated torque.

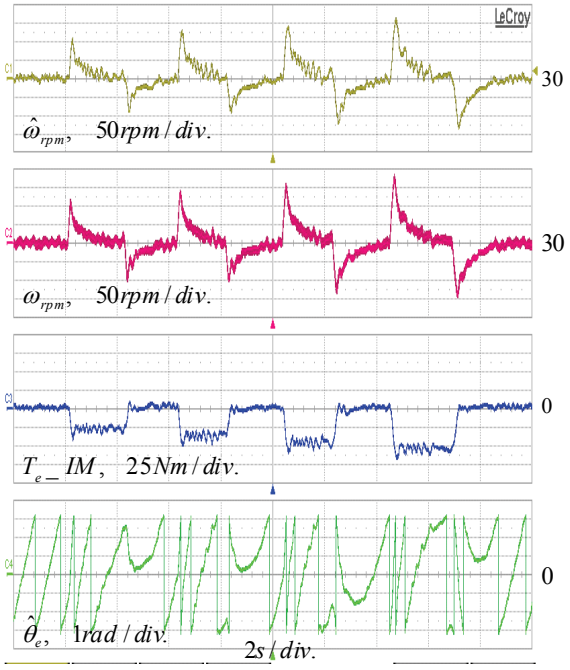

Fig. 6 Experimental result under load variations at the constant speed, 30 r/min.

Fig. 5 shows the performance of the sensorless speed control under slow speed reference variation near zero speed with the rated torque. The speed reference was slowly changed from 100 r/min to -100 r/min and vice versa. The slew rate was 10 (r/min)/s. $\hat{\theta}_e$ has some distortions due to the multiple saliencies. This distortion produces the ripple of $\hat{\omega}_{rpm}$ and it would result in the ripple of the torque of IM denoted as T_e_IM .

Fig. 6 shows the waveforms under load variation. The load torque was applied from 50 % to 100 % of the rated torque in the step manner at the constant speed, 30 r/min. Each load is -30, -40, -50 and -60 Nm, respectively. Fig. 7 shows the similar waveforms under zero speed.

Fig. 8 shows the waveforms when the synchronous frequency is zero. The load torque was applied as 44 Nm at the constant speed of -20 r/min. Because of the negative rotating speed and positive slip speed for the positive torque, the angular speed of the rotor flux linkage is null. Fig. 9 shows the similar waveforms with 40 Nm and 50 Nm. For the simplicity, $\hat{\omega}_{rpm}$ and ω_{rpm} are omitted. Under no load condition, $\hat{\theta}_e$ of three figures are identical. When loads are applied, the frequencies of $\hat{\theta}_e$ are slightly different from each other due to their slip frequencies. The frequencies of $\hat{\theta}_e$ are 0 Hz, -0.07 Hz and 0.1 Hz, respectively.

Based on these experimental results in figures, it can be concluded that the proposed method is robust over all loads

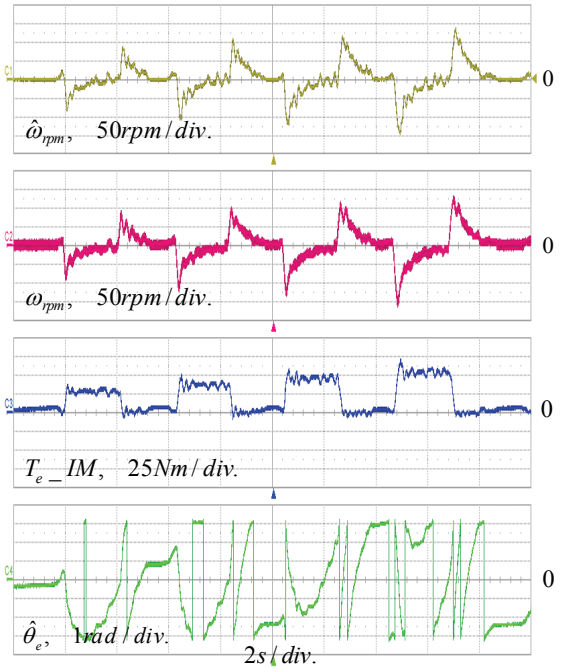

Fig. 7 Experimental result under load variations at zero speed

and reveals reasonable performance at low frequency including zero.

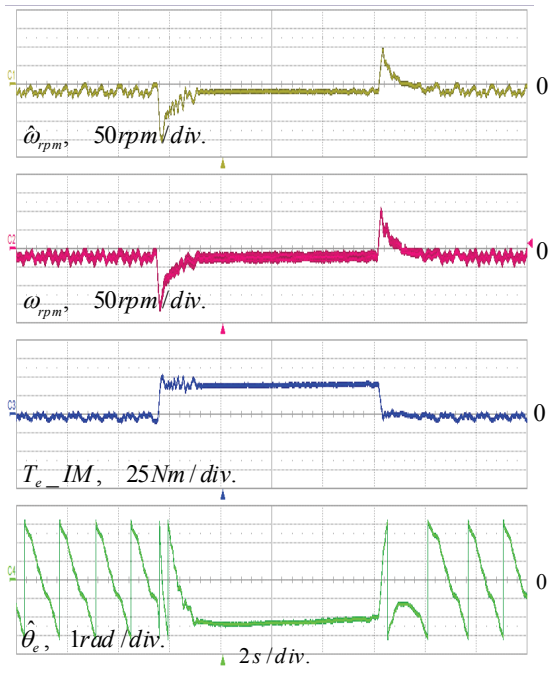

Fig. 8 Experimental result under zero synchronous frequency (44 Nm was applied at the constant speed of -20 r/min.)

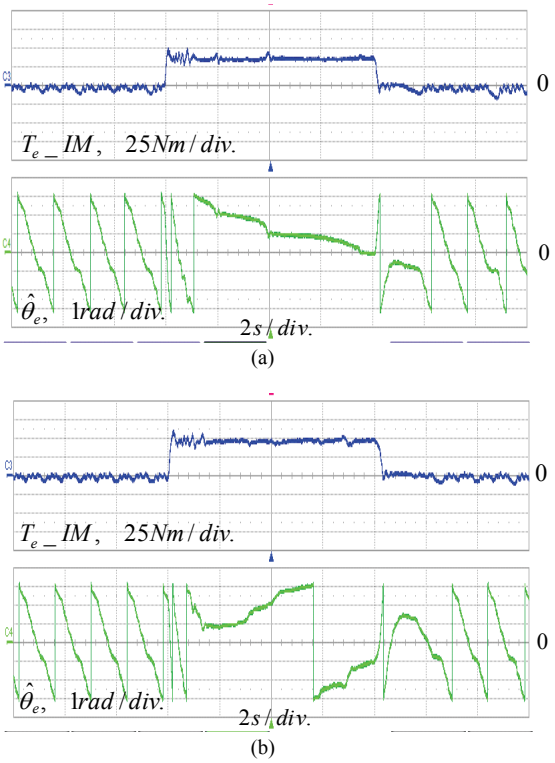

Fig. 9 Experimental result near zero synchronous frequency: (a) 40 Nm and (b) 50 Nm were applied at the constant speed of -20 r/min.

V. CONCLUSIONS

This paper presents a sensorless control method for induction machines based on a square-wave voltage injection into q axis. The multiple saliency problems can be overcome by injecting square-wave signal into the estimated synchronous reference frame. By injecting the square-wave signal into q axis, the robustness of the estimation of the position of the rotor flux against load condition and operating speed is enhanced. And, the variation of the characteristics of the saliency can be easily compensated by a linear function of q axis current. The experimental results show reasonable performances under the slow speed reference variation near zero speed and under the load torque disturbance including zero frequency.

VI. REFERENCES

[1] M. Tursini, R. Petrella, and F. Prasiliti, "Sensorless control of an IPM synchronous motor for city-scooter application," *Conf. Rec. of IEEE IAS. Annu. Meet.*, Oct. 2003, pp. 1472-1479.

[2] K. Ide, M. Takaki, S. Morimoto, Y. Kawazoe, A. Maemura and M. Ohto, " Saliency-based sensorless drive of adequate designed IPM motor for robot vehicle application," *in conf. rec. of PCC*, pp. 1126-1133, April 2007.

[3] S. Ogasawara and H. Akagi, "An approach to position sensorless drive for brushless dc motor," *IEEE Trans. Ind. Applicat.*, vol. 27, pp. 928-933, Sept./Oct. 1991.

[4] S. Ogasawara and H. Akagi, "Implementation and position control performance of a position-sensorless IPM motor drive system based on magnetic saliency," *IEEE Trans. Ind. Applicat.*, pp. 806-812, July/Aug. 1998.

[5] S. I. Yong, J. W. Choi and S. K. Sul , " Sensorless Vector Control of Induction Machine Using High Frequency Current Injection " , in Conf. Rec. IEEE-IAS Annu. Meeting, 1994.

[6] P. L. Jansen and R. D. Lorenz, "Transducerless position and velocity estimation in induction and salient AC machines," *IEEE Trans. Ind. Applicat.*, vol. 31, pp. 240-247, Mar./Apr. 1995.

[7] J. I. Ha and S. K. Sul, "Sensorless field-orientation control of an induction machine by high-frequency signal injection," *in Conf. Rec IEEE-IAS Annu. Meeting, 1997*.

[8] M. J. Corley and R. D. Lorenz, "Rotor position and velocity estimation for a permanent magnet synchronous machine at standstill and high speeds," *in Conf. Rec. IEEE-IAS Annu. Meeting*, vol. 1, 1996, pp. 36-41.

[9] J. H. Jang, S. K. Sul, J. I. Ha, K. Ide, and M. Sawamura, "Sensorless drive of surface-mounted permanent-magnet motor by high-frequency signal injection based on magnetic saliency," *IEEE Trans. Ind. Applicat.*, vol. 39, pp. 1031-1039, July/Aug., 2003.

[10] Y. D. Yoon, S. K. Sul, S. Morimoto and K. Ide, "High bandwidth sensorless algorithm for AC machines based on square-wave type voltage injection," in *Conf. Rec. IEEE ECCE*, 20-24 Sep. 2009, pp. 2123-2130.

[11] R. Leidhold and P. Mutschler, "Improved method for higher dynamics in sensorless position detection," in *Conf. Rec. IECON*, 10-13 Nov. 2008, pp. 1240-1245.

[12] M. W. Degner and R. D. Lorenz, "Using multiple saliencies for the estimation of flux, position, and velocity in AC machines," *IEEE Trans. Ind. Applicat.*, vol. 34, pp. 1097-1104, Sept./Oct. 1998.

[13] C. Caruana, G.M. Asher, and M. Sumner, "Performance of HF signal injection techniques for zero-low-frequency vector control of induction Machines under sensorless conditions," *IEEE Trans. Ind. Electron.*, Vol. 53, pp. 225-238, Feb. 2006.

[14] P. L. Jansen and R. D. Lorenz, "Transducerless field orientation concepts employing saturation-induced saliencies in induction machines," *IEEE Trans. Ind. Appl.*, vol. 32, no. 6, pp. 1380-1393, Nov./Dec. 1996.